

HOSTED BY



Contents lists available at ScienceDirect

Journal of King Saud University – Science

journal homepage: [www.sciencedirect.com](http://www.sciencedirect.com)

Original article

# Synthesis, TD-DFT, and optical properties study of a chromeno-quinoline (acceptor) and mirror-less laser action enabled by energy transfer from a conjugated-polymer (Donor)



Saradh Prasad <sup>a,b</sup>, Mohamad S. Alsalhi <sup>a,b</sup>, Raju Suresh Kumar <sup>c,\*</sup>, Abdulrahman I. Almansour <sup>c</sup>, Natarajan Arumugam <sup>c</sup>, Manal Fahad Alkaltham <sup>c</sup>, Khlood Ibrahim Al-Shemaimari <sup>c</sup>, Haya bint Abdulaziz Al-Tamimi <sup>a</sup>

<sup>a</sup> Department of Physics and Astronomy, College of Science, King Saud University, 11451 Riyadh, Saudi Arabia

<sup>b</sup> Research Chair on Laser Diagnosis of Cancers, Department of Physics and Astronomy, College of Science, King Saud University, 11451 Riyadh, Saudi Arabia

<sup>c</sup> Department of Chemistry, College of Science, King Saud University, P.O Box 2455, Riyadh 11451, Saudi Arabia

## ARTICLE INFO

### Article history:

Received 5 June 2022

Revised 26 June 2022

Accepted 29 July 2022

Available online 3 August 2022

### Keywords:

Chromenoquinolines

MCQ

PFOPX

Energy transfer

FRET

ASE

## ABSTRACT

Structurally interesting chromeno-quinolines were constructed via the cyclization reaction of *O*-propargylated naphthaldehyde and substituted anilines in good yields. We explored compound methyl-chromenoquinoline (MCQ) in detail for its optical properties using Time-dependent density-functional theory (TD-DFT) and experimental studies. The conjugated-polymer (CP) Poly[(9,9-dioctylfluorenyl-2,7-diyl)-co-(2,5-p-xylene)] or [(ADS145UV or PFOPX)] was studied as donor. The TD-DFT implied that MCQ is a fluorescent compound with well-defined highest occupied molecular orbital (HOMO) and lowest unoccupied molecular orbital (LUMO) structure at  $-5.327$  eV and  $-1.836$  eV, respectively, with an energy gap of 3.49 eV in toluene captivity. The TD-DFT-based model and experimental study showed an energy gap of 3.326 eV and 3.351 eV, respectively, and the deviation was 0.025 eV. The experimental studies of MCQ showed solvent-dependent fluorescence peak shifted from  $445 \pm 2$  nm to  $538 \pm 2$  nm for dielectric constant ranging from 0.01 (hexane) to 10.2 (water). Despite the good optical properties, MCQ produced a weak laser-induced fluorescence (LIF) and not produce amplified spontaneous emission (ASE) to any pump energy of 3rd harmonic from Nd:YAG laser (5 ns, 355 nm). When PFOPX of concentration 500 nM (500  $\mu$ L) was added to MCQ of 506 mM (3.5 mL) concentration, the LIF suddenly improved tenfold due to efficient Fluorescence resonance energy transfer (FRET) process. At the optimal concentration of PFOPX (670 nM) in MCQ solution, the spectrum changed dramatically. The spectrum has five peaks with a LIF in the background, where peaks around 393.5 nm and 417.3 nm attribute to the oligomer; 438.7 nm attributed to a combined fluorescence of PFOPX and MCQ; 466.4 nm, and 493.1 nm corresponding to MCQ. Analysis shows that the peaks at 440 nm (partly) and 493 nm were ASE from MCQ.

© 2022 The Author(s). Published by Elsevier B.V. on behalf of King Saud University. This is an open access article under the CC BY-NC-ND license (<http://creativecommons.org/licenses/by-nc-nd/4.0/>).

## 1. Introduction

Chromene structural moieties are one of the most vital classes of the heterocyclic units with diverse biological activities

\* Corresponding author.

E-mail address: [sraju@ksu.edu.sa](mailto:sraju@ksu.edu.sa) (R.S. Kumar).

Peer review under responsibility of King Saud University.



(Alizadeh et al., 2008; Cho et al., 2008; Conti and Desideri, 2009; Kjer et al., 2009; Nicolaou et al., 2000; Tangmou et al., 2006). These structural moieties have also been used as eco-friendly agrochemicals, pigments, and essential intermediates in constructing various natural products (Chang and Grubbs, 1998; Kleschick and Heathcock, 1978; Minami et al., 1978; Wang and Finn, 2000). Quinolines, another class of heterocyclic units, are known for their diverse applications, and there has been substantial attention in the synthesis of derivatives of quinolines (Balasubramanian and Keay, 1996; Campbell, 1976). The hybridization of chromene and quinoline structural moieties in a single molecule would be expected to enhance its activity as these derivatives have attracted

<https://doi.org/10.1016/j.jksus.2022.102260>

1018-3647/© 2022 The Author(s). Published by Elsevier B.V. on behalf of King Saud University.

This is an open access article under the CC BY-NC-ND license (<http://creativecommons.org/licenses/by-nc-nd/4.0/>).

much attention recently. Chromenoquinolines (CQs) are an important class of heterocyclic compounds with applications in diverse fields (Geng et al., 2018). CQs were found to be useful as selective progesterone receptors (Zhi et al., 2003), transcriptional activity (Coghlan et al., 2001), glucocorticoid modulators (Ku et al., 2003), and estrogenic agents (Vu et al., 2007). CQs attracted the attention of chemists owing to their remarkable and versatile properties. In response, the chemical society paid considerable interest in developing strategies for synthesizing their derivatives, which are also known for their biological potential. However, the fluorescence properties of these derivatives are rarely explored for the design of fluorescent sensors (Kand et al., 2012).

Most of the CQs were used as fluorescent probes. A fluorescent probe based on methylated CQ dissolved in water was used to detect thiophenol. CQ with a sensing moiety of  $\beta$ -chlorovinyl aldehyde was used as a two-photon (TP) imaging probe to monitor  $\text{SO}_2$  in the biological environment (Cai et al., 2019). Live cell imaging and cell permeability of thiols were performed using a chromenoquinoline probe (Qiao et al., 2022). Methylated CQ was used for mitochondrial labeling (Liu et al., 2018). CQ was not reported to produce a laser despite its excellent optical properties.

Energy transfer plays an important role in biophysical applications such as protein interactions (Kenworthy, 2001), membrane fluidity (Ghatak et al., 2011), protein conformation (Heyduk, 2002) and chemosensory applications (Bayraktutan et al., 2022). Forster resonance energy transfer (FRET), is the most important energy-transfer mechanism. It is analog to wireless charging; an excited donor resonantly transfers energy using the dipole-dipole moment to an acceptor (Clegg, 1995). This technique is an excellent tool for developing an energy transfer-based laser from molecules otherwise hard to produce (Cerdán et al., 2012). The FRET process can be employed to induce ASE from inefficient material using a suitable donor. The conjugated materials are very efficient donors.

A yellow oligomer produced ASE with help FRET energy transfer from donor oligomer; the former would not produce laser action without the energy transfer process (Aljaafreh et al., 2019). A rare radiative type energy transfer was observed between an oligomer and conjugated polymer (Aljaafreh et al., 2021a; Prasad et al., 2020). The energy transfer between a perovskite quantum dot as acceptor and an oligomer as a donor was reported earlier (Aljaafreh et al., 2021c,b). Conjugated polymers are very efficient laser materials (Alfahd et al., 2017), and it is compatible with MCQ since both are highly soluble in non-polar solvents.

In this context and in continuation of our research interest in the synthesis of novel small molecules for laser applications, in the present work, we report an efficient synthesis of CQs employing a mixture of CuI and  $\text{La}(\text{OTf})_3$  as the catalyst. Among the synthesized compounds, the MCQ (5b) showed the best optical, energy transfer and laser property. Therefore, we extensively studied the properties of compound MCQ. The TD-DFT, optical properties, solvent-based fluorescence, and laser action from MCQ using FRET type energy transfer from a UV-violet emitting conjugated-polymer PFOPX. We studied MCQ in detail for its optical properties using TD-DFT and experimental. The conjugated-polymer (CP) Poly[(9,9-dioctylfluorenyl-2,7-diyl)-co-(2,5-p-xylylene)] or [(ADS145UV or PFOPX)] was studied as donor. The TD-DFT implied that MCQ is a fluorescent compound with well-defined highest occupied molecular orbital (HOMO) – lowest unoccupied molecular orbital (LUMO) structure. The triple monomer-based oligomer with a truncated tail model of PFOPX was used for TD-DFT studies. The TD-DFT-based model and experimental studies were utilized to estimate the accurate energy gap. The experimental studies of MCQ showed fluorescence peak shift depending on solvent polarity. Despite the good optical properties, MCQ produced a weak laser-induced fluorescence (LIF) and did not produce amplified

spontaneous emission (ASE) for a pump wavelength of 355 nm. The intensity of LIF improved multifold when a drop of PFOPX was added to MCQ. At the optimal concentration of PFOPX (670 nM) in MCQ solution, the spectrum changed dramatically. The spectrum has five sharp peaks with a LIF in the background, where peaks around 393.5 nm and 417.3 nm attribute to the oligomer; 438.7 nm attribute to a combined oligomer fluorescence and MCQ; 440.4 nm, and 493.1 nm ASE peaks corresponding to MCQ. To the best of our knowledge, this could be the first report on a mirror-less laser from MCQ using energy transfer from PFOPX.

## 2. Materials and method

### 2.1. Materials

The common name of MCQ is 11-methyl-8H-benzo[5,6]chromeno[4,3-b]quinoline and its molecular structure is shown in Fig. 1(a). It has a molecular weight of  $297.357 \text{ g mol}^{-1}$ .

The donor used in this study is a conjugated co-polymer called Poly[(9,9-dioctylfluorenyl-2,7-diyl)-co-(2,5-p-xylylene)] or [(ADS145UV or PFOPX). PFOPX the molecular structure is shown in Fig. 1(b) and has an average molecular mass of  $47,500 \text{ g mol}^{-1}$  and is sourced from company called American dye source, Baie-d'Urfé, Quebec Canada. Solvents such as hexane, toluene, benzene, chloroform, acetone, and ethanol were sourced from Sigma Aldrich, and deionized (DI) water was sourced from King Saud University.

### 2.2. Methods

#### 2.2.1. Synthesis

General procedure for the synthesis of CQs is as follows considering a representative example 5b. To a mixture of O-propargylated naphthaldehyde 0.100 g (0.476 mmol) and p-methylaniline 0.051 g (0.476 mmol) in acetonitrile (15 mL), was added CuI 0.005 g (10 mol%) and  $\text{La}(\text{OTf})_3$  0.014 g (10 mol%) and refluxed for 5 hrs. After completion of the reaction as indicated by TLC, the excess acetonitrile was removed under vacuum, and 20 mL of water was added to the reaction mixture. The aqueous layer was extracted with dichloromethane, and the combined organic layers were dried over anhydrous  $\text{Na}_2\text{SO}_4$ , filtered and concentrated under reduced pressure. The crude product was purified using hexane and ethyl acetate to furnish the pure product in good yield (89 %) by column chromatography.

#### 2.2.2. Experimental setup

Spectrophotometric measurements were conducted at room temperature using a Perkin Elmer Lambda 950 spectrophotometer (Llantrisant, United Kingdom) for absorption spectra, and emission spectra were obtained using a spectrofluorometer (LS 55, Llantrisant, United Kingdom). A 5 cm focal length quartz cylindrical lens was used to focus the pump pulse from the Nd:YAG laser into the MCQ and PFOPX solutions for transverse optical pumping. The pump pulse from the Nd:YAG laser was focused into the MCQ, PFOPX, and mixture solutions by a frequency tripled Nd:YAG (355 nm and 5 ns pulses). These solutions produced laser-induced fluorescence (LIF) and ASE under suitable pump energies.

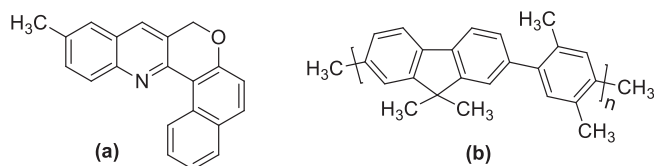


Fig. 1. Molecular structure of (a) MCQ and (b) PFOPX.

To record spectral profiles, the output emission was connected to an optical fiber linked to a spectrograph with a linear array charge-coupled device (LA-CCD) from Ocean Optics Spectroscopy (Maybachstrasse, Ostfildern, Germany).

### 2.2.3. Computational setup

All simulations were done using TD-DFT were done using Gaussian 16 software (Frisch et al., 2016) in a workstation with AMD Ryzen 9 5950X, with 128 GB RAM, 16-core, 32-threads, 1 TB M.2 SSD (Aljaafreh et al., 2021b). The MCQ calculations were done without any approximation or cutting of the molecular structure. However, to simulate TD-DFT of PFOPX, the computation hardware required may be overwhelming and time-consuming. Hence, a close approximation called the oligomer model was followed to investigate the TD-DFT of macromolecule PFOPX. Specifically, we used three monomer units with a truncated tail from (9,9-dioctyl) to (9,9-dimethyl), since the tail's contribution to the HOMO – LUMO structure was low (Aljaafreh et al., 2021b; McCormick et al., 2013). We calculated TD-DFT for a number of monomer units from 1 to 4, and HOMO-LUMO gaps were plotted against (1/n); the extrapolation gives the energy gap of the CP (Civcir et al., 2020).

## 3. Results and discussion

### 3.1. Chemistry

In the current research work, the starting precursor O-propargylated naphthaldehyde was synthesized from 2-hydroxy-1-naphthaldehyde and propargyl bromide following the literature procedure (Yadav et al., 2018). The reaction of O-propargylated naphthaldehyde and anilines with 10 mol% each CuI and La(OTf)<sub>3</sub> in acetonitrile under reflux for 5 h afforded the products (5a-e) in good yields (80–92 %) (Scheme 1).

Characterization of the synthesized CQs was done considering a representative compound 5b. In the <sup>1</sup>H NMR spectrum, the singlet at 2.51 ppm is assigned to the methyl group while the methylene protons appeared as a singlet at 5.31 ppm. The aromatic protons resonated as doublets and multiplets around 7.25–9.95 ppm. Other CQs (5a, 5c-e) were also analyzed based on similar considerations. All the synthesized compounds 5a-e are in accordance with their literature data (Sami et al., 1992; Sharghi et al., 2013).

Synthesis of compound 5a by Sami et al. (1992) involved the reaction of 1-chloro-3H-benzochromene-2-carbaldehyde and anilines in ethanol in the presence of 2 N hydrochloric acid at room temperature to afford enaminoimine hydrochlorides, which upon heating underwent ring closure with the elimination of one equivalent of arylamine hydrochloride to afford the chromenoquinoline 5a, 5b, 5c, and 5d respectively in 48 %, 42 %, 33 %, and 39 % yields respectively. Ramesh et al. (2010) reported the synthesis of com-

pound 5a in 78 % yield from O-propargyl-1-naphthaldehyde and aniline. Compound 5e, reported by Sharghi et al. (2013) involved the reaction of O-propargyl-1-naphthaldehyde and aniline using a heterogeneous metal catalyst.

The probable mechanism for the formation of CQs 5 is shown in Scheme 2. The O-propargylated naphthaldehyde reacts with arylamines to afford the intermediate imine 6, which then undergoes a formal [4+2] cycloaddition to form the intermediate 7. The dihydroquinoline intermediate 8 derived from 7, on air oxidation furnishes the CQs 5.

### 3.2. Computation studies

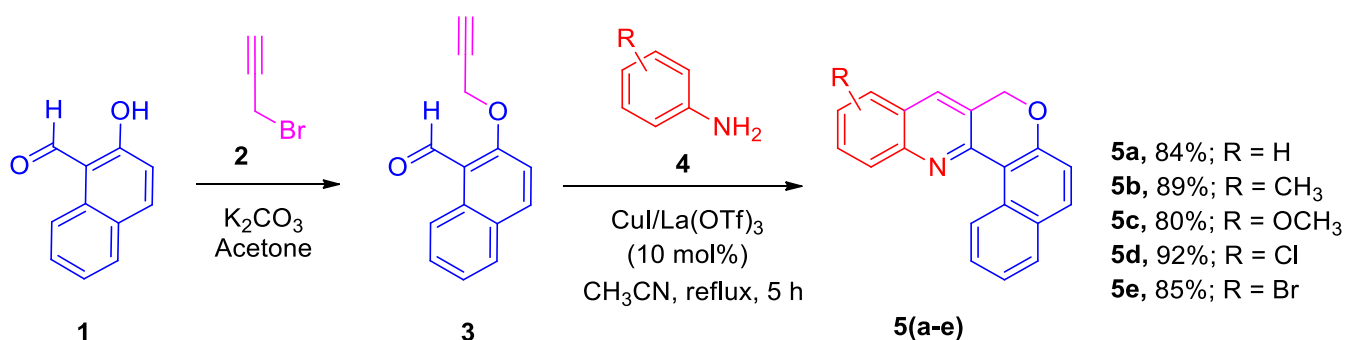
The computational studies of MCQ and PFOPX were calculated using TD-DFT Becke, 3-parameter, Lee–Yang–Parr (B3LYP) function with 6–31G\*(d,p) basis set and discussed in the section. The standard color scheme of furrier densities was followed with a transparency of 50 % to show the molecular structure.

#### 3.2.1. TD-DFT of MCQ (Acceptor)

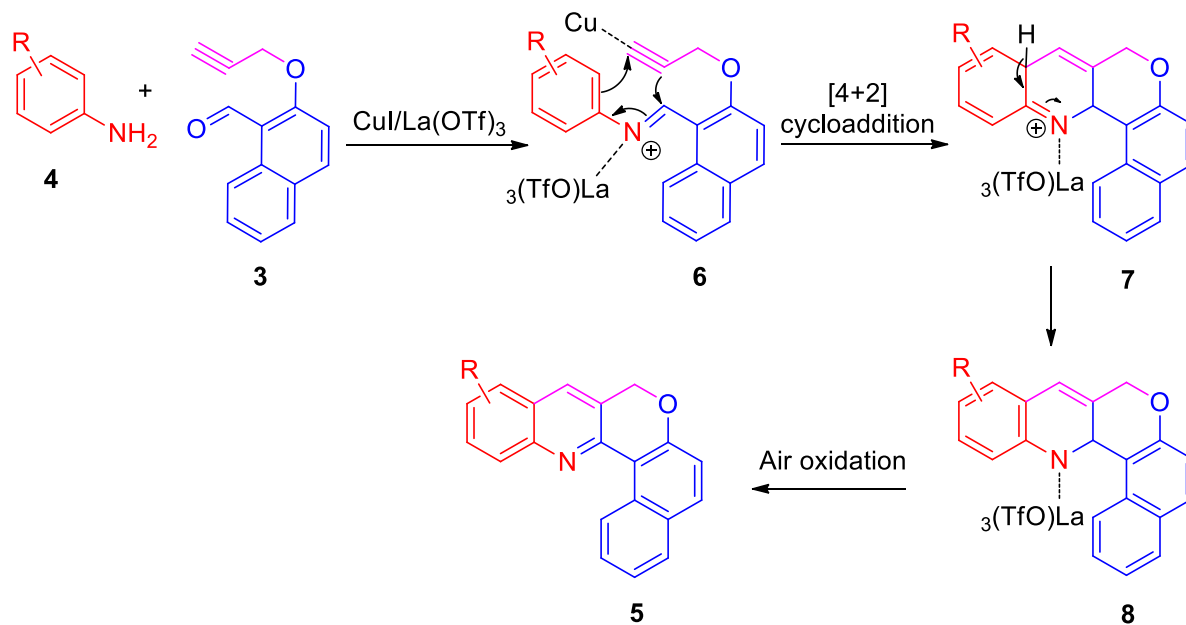
The molecular orbitals (HOMO-LUMO) structure of the MCQ in toluene cavitation calculated using TD-DFT with B3LYP/6-31G\* bases set is depicted in Fig. 2(a). The contour of HOMO is the same in the acetone when compared to toluene. The orbital densities of HOMO orbital densities were present throughout the core structure. However, more on the left side. On the other hand, the LUMO is spread throughout the core structure of the MCQ, with more densities accumulated on the right side. The calculated bandgap was 3.49 eV, where the HOMO was located at –5.32 eV, and LUMO was located at –1.836 eV. The computed UV–vis spectrum is consistent with experimental results of MCQ in the toluene as in Fig. 2 (b), showing three peaks 334.6 nm, 348.9 nm, and 408.6 nm. In comparison, the experiment results revealed that are two peaks at 327 nm and 410 nm; and a shoulder around 353 nm for MCQ in toluene (For low concentration), which could be attributed to S<sub>0</sub>-S<sub>3</sub> (Peak), S<sub>0</sub>-S<sub>2</sub> (shoulder), and S<sub>0</sub>-S<sub>1</sub> (Peak) vibrational band respectively (Duan et al., 2020). The discrepancy between simulations and experimental is due to the concentration effect. Fig. 2(c) shows the ECD spectrum of MCQ shows three Δε at the same oscillator strengths of UV–vis spectra and with –0.0069, 0.00318, and –0.0341 (10<sup>-40</sup> esu<sup>2</sup> cm<sup>2</sup>). And it has a positive and negative cotton effect, which is essential for the polarizability of the MCQ. The absorption spectra have three peaks at wavelengths 338.7 nm, 356.6 nm, and 422.2 nm with oscillator strengths of 0.1039, 0.0017, and 0.2866 (10<sup>-40</sup> esu<sup>2</sup> cm<sup>2</sup>), respectively.

#### 3.2.2. TD-DFT of PFOPX (Donor)

The PFOPX (donor) is a macromolecule; the TD-DFT of monomer is alone discussed here, although calculations were done for few monomers (oligomer) model i.e. n = 1, 2, 3 and 4. Fig. 3(a)



Scheme 1. Synthesis of CQs, 5(a-e).



**Scheme 2.** Mechanism for the formation of CQs, 5.

shows the orbit densities of PFOPX ( $n = 1$ ) for HOMO, and LUMO calculated using TD-DFT B3LYP method with 6-31G\*(d,p) basis set. The LUMO of simulated PFOPX for monomer units  $n = 1, 2, 3$  and 4 tended to become proximity to the simulated LUMO of MCQ, which could be attributed modulation of the HOMO and LUMO of the mixture solution and energy transfer from PFOPX to MCQ.

Fig. 3(b) shows the UV-vis spectra of PFOPX ( $n = 1$ ) using the TD-DFT B3LYP method with a 6-31G\*(d,p) basis set. This indicates that this material has a positive and negative cotton effect, which is essential for the polarizability of the PFOPX. The absorption spectra have three peaks at wavelengths 310.2 nm, 277.4 nm, and 266.92 nm, with oscillator strengths of 1.226, 0.0038, and 0.0213 ( $10^{-40}$  esu<sup>2</sup> cm<sup>2</sup>), respectively. The energy gap of the donor was around 4.35 eV. The LUMO and HOMO of the donor were located at  $-0.931$  eV and  $-5.366$  eV, respectively.

The estimated bandgap using oligomer model simulation up to  $n = 4$  plotted against the inverse of repetitive monomer units, and extrapolation up to  $n$  tends to infinity ( $n \rightarrow \infty$ ) molecular (Civcir et al., 2020; Gopalakrishnan et al., 2018). It is compared with experimentally estimated using the intersection of absorption and fluorescence spectra method (green star) is depicted in Fig. 4. The difference between the calculated and experimental energy gap is 0.036 eV, hence the simulated HOMO – LUMO structures and locus of the energy levels are very reliable. This is a crucial step in understanding the energy transfer dynamics that allows MCQ to improve the spectral intensity and band narrowing and produce dual ASE discussed later.

### 3.3. Experimental studies

#### 3.3.1. Absorption spectra of MCQ in toluene

Toluene is the best solvents based on quantum yield, the quantum of MCQ in different solvent was calculated using Eq. (1) (section 3.3.4) and given in Table 1. Hence, we studied the different concentrations of MCQ in toluene was studied.

Fig. 5 shows the absorption spectra of MCQ in toluene for concentrations ranging from 52  $\mu$ M to 1.68 mM. For concentrations above 1.68 mM, the absorption spectra were saturated. The spectral profile remained the same. Only a minimal shift in the spectral

peaks were observed. All spectra had three standard features at 338.7 nm, 356.6 nm (shoulder) and 422.2 nm corresponding to vibrational bands of  $S_0-S_3$ ,  $S_0-S_2$ , and  $S_0-S_1$ , and it is consistent with TD-DFT results with a small discrepancy.

#### 3.3.2. Fluorescence spectra of MCQ.

Fig. 6(a), shows the fluorescence spectra of MCQ in toluene for concentrations ranging from 105  $\mu$ M to 13.4 mM; the fluorescence increases with an increase in concentration for low concentration up to the optimal concentration of 841  $\mu$ M, where it attains the peak intensity. The fluorescence spectral profile showed a peak and a shoulder at 472 nm and 498 nm, respectively, for concentration 841  $\mu$ M. Above this concentration, the fluorescence decreases with increased concentration, which could be attributed partly to increased reabsorption and vibronic band damping at higher concentrations (Aljaafreh et al., 2021a, 2019; Prasad et al., 2020). The rise in concentration also redshifts the fluorescence peak from 460 nm to 493 nm for concentrations 105  $\mu$ M to 13.4 mM. The MCQ also showed a significant Stokes shift of 78 nm for a solution concentration 841  $\mu$ M, as shown in Fig. 6(b).

#### 3.3.3. Effects of solvent polarity

The MCQ was dissolved with good solubility in most solvents. The solution becomes cloudy in a high polar solvent and clear greenish-yellow in non-polar and medium polar solvents. Intrigued by this behavior, we tested MCQ in solvents with increasing polarity from non-polar to highly polar solvent. The concentration of MCQ was kept constant at 850  $\mu$ M for all solvents. It showed a redshift in fluorescence peak depending on the increase in the polarity of the solvent environment, as shown in Fig. 9 when the polarity of solvent was 0.12 (hexane), the fluorescence peak was 445.8 nm. Similarly, when the polarity of solvent subsequently increased to 2.4, 2.7, 4.12, 5.12, 5.26, and 10.22 using toluene, benzene, chloroform, acetone, ethanol, and water solvents shifted the fluorescence peak of MCQ to 481 nm, 483 nm, 495 nm, 508 nm, 513 nm, and 538 nm respectively as illustrated in Fig. 7. The redshift (Lakshmidevi et al., 2017) of MCQ due to reduction of the energy gap could be attributed to increased solvent polarity (Brugel and Williams, 1993) and it is observed in organic molecules such as oxazone (Bani-Yaseen and Al-Balawi, 2014), nifenazone

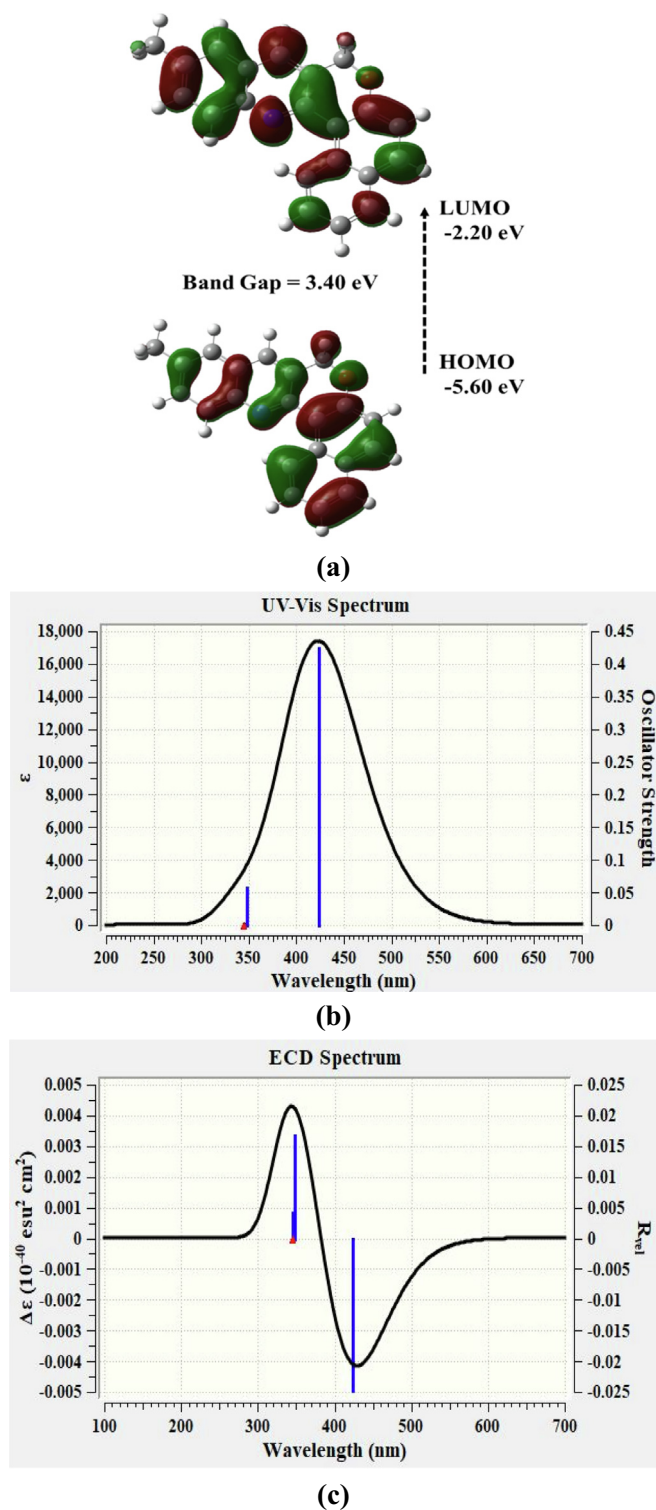


Fig. 2. (a) Molecular orbitals Structure of MCQ simulated using TD-DFT B3LYP method with 6-31G\*(d,p) basis set. (b) Simulated US-VIS and (c) ECD spectra of MCQ using TD-DFT B3LYP method with 6-31G\*(d,p) basis set.

(NIF), a pyrazole-nicotinamide drug (Hrdlovic et al., 2010) and Bichromophoric Coumarins (Clegg, 2009).

### 3.3.4. Fluorescence quantum yield

The fluorescence quantum yield (QY,  $\phi$ ) of MCQ in toluene was measured by using the Equation (1):

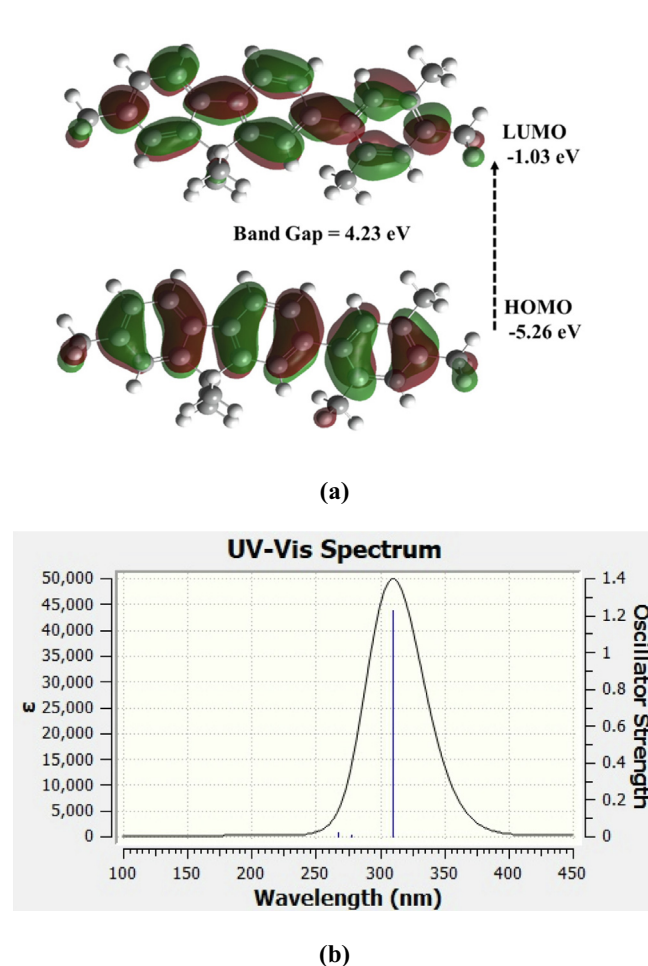


Fig. 3. (a) Simulated molecular orbitals structure (Fourier densities) and (b) UV-vis and of PFOPX using TD-DFT B3LYP method with 6-31G\*(d,p) basis set.

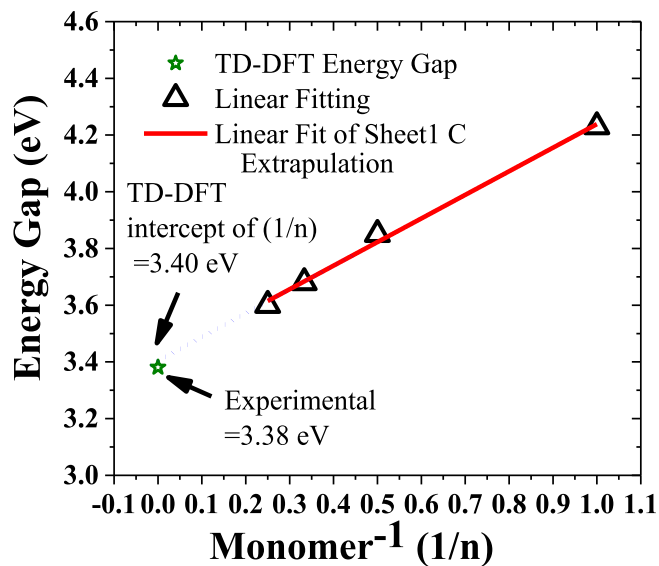
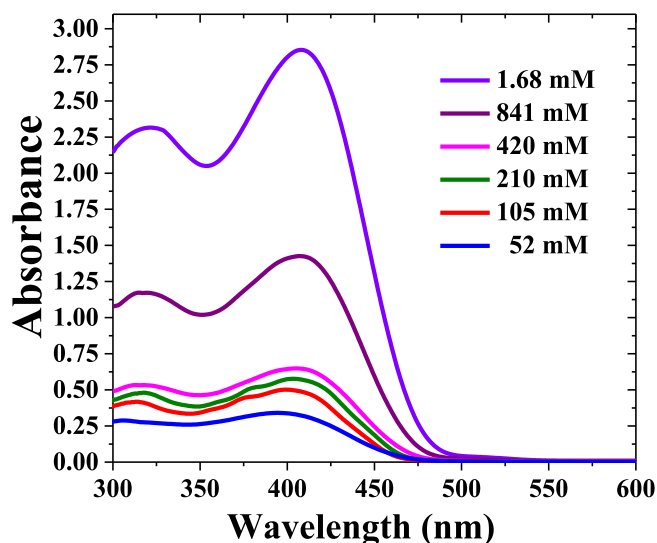


Fig. 4. Estimated bandgap using oligomer modeling of PFOPX for monomer reputation units up to  $n = 3$  plotted against the inverse of repetitive monomer units, and extrapolation up to  $n$  tends to infinity ( $n \rightarrow \infty$ ) molecular, and compared with experimentally estimated using the intersection of absorption and fluorescence spectra method (green star).

**Table 1**  
The quantum yield (Q.Y), Stokes shift, absorption peak, and fluorescence peak of MCQ under different solvent environment.

Solvent	Q.Y (%)	Stokes shift (nm)	Absorption peak (nm)	Fluorescence peak (nm)
Hexane	12.7 %	66	380	446
Toluene	20.8 %	78	405	483
Benzene	18.2 %	62	422	484
Chloroform	14.3 %	59	436	495
Acetone	11.2 %	67	441	508
Ethanol	8.1 %	55	458	513
Water	5.2 %	49	489	538



**Fig. 5.** Absorption spectra of MCQ in toluene for different concentrations ranging from 52 μM to 1.68 mM.

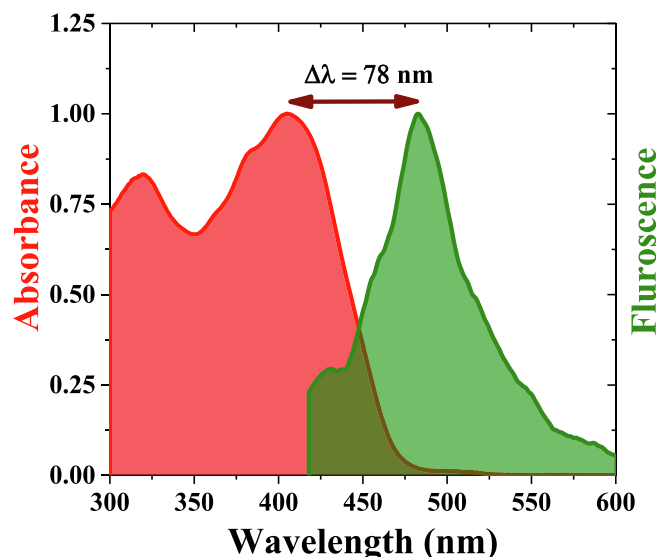


**Fig. 6b.** The Stokes' shift between absorption and fluorescence Peak of MCQ.

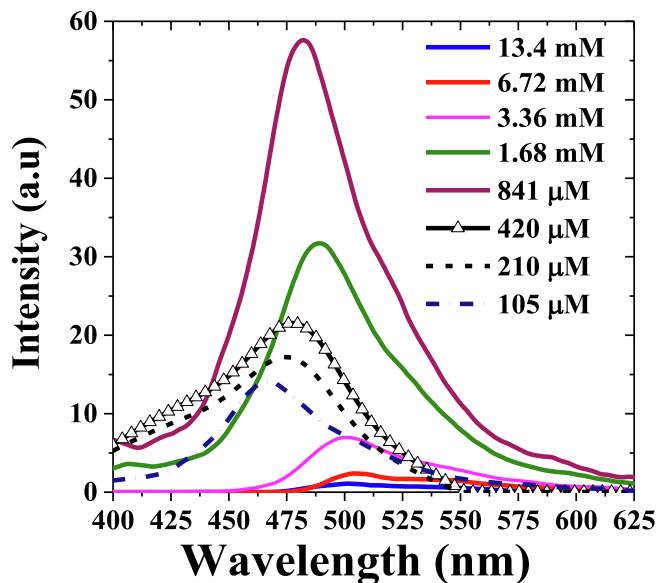


**Fig. 6a.** Fluorescence spectra of MCQ in toluene for different concentrations.

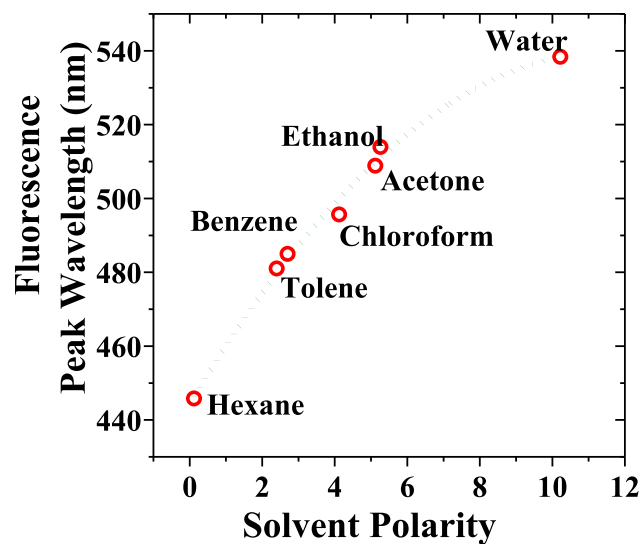


**Fig. 7.** The fluorescence peak with respect to the solvent polarity. The increase in polarity of the solvent results in a peak's redshift.

$$\Phi_F(s) = \Phi_F(R) \left[ \frac{\int I_S(\bar{\nu}) d\nu}{\int I_R(\bar{\nu}) d\nu} \times \frac{A_R}{A_s} \times \frac{n_s^2}{n_R^2} \right] \quad (1)$$

The integral over I represents the area under the fluorescence spectrum, and the indices S and R are the sample and reference,

respectively. A is the optical density of the MCQ in toluene (in this case), and n is the refractive index of the toluene.  $\phi_F(R)$  is the reference fluorophore, and it is coumarin dissolved in toluene with QY of (78 %). The QY of MCQ is found to be 20.76 % (at maximum fluorescence response concentration 841 μM). The QY and Stokes' shift of MCP in different solvent is given in [Table 1](#).

### 3.3.5. Absorption and fluorescence spectra of donor (PFOPX)

Despite the best efforts to pump the MCQ in toluene using 3rd harmonics of Nd:YAG laser (355 nm) at very high pump power and concentration, it only produced LIF, hence a donor (PFOPX) was introduced at very low concentration to improve the performance of the MCQ. At the low concentration comparable to relative concentration in the mixture solution, PFOPX would not produce ASE; it required a minimum concentration to produce ASE. But such low concentration PFOPX was sufficient to produce energy transfer and made MCQ produce dual ASE. Fig. S1 shows the absorption spectra have a peak around 340 nm, and Fig. S2 shows the fluorescence spectra have two peaks around 393 nm and 415 nm and a shoulder around 450 nm.

### 3.3.6. Energy transfer and laser spectra

As the molecules in a ground state are pushed to an excited state by the incoming photon. These molecules remain in an excited state for a few nanoseconds. There is a high probability that energy transfer will occur resonantly when an acceptor molecule is spaced less than 10 nm called Förster radius ( $\leq 10$  nm) for an effective energy transfer, also known as Förster-type resonant energy transfer (FRET) (Belušáková et al., 2017; Clegg, 1995; Hussain, 2009).

Fig. 8 illustrates the emission-absorption cross-section about 91.6 % of conjugated polymer PFOPX's fluorescence (Donor) overlaps with MCQ (Acceptor) absorption spectra. Hence there is the abundant probability for energy transfer between PFOPX and MCQ. However, the critical factor for energy transfer is the Förster transfer radius ( $R_0$ ).  $R_0$  can be calculated using the following equation:

$$R_0^6 = \frac{9000(\ln 10)k^2\phi_D}{128\pi^5n^4N_0} \int \frac{F_D(\bar{\nu})\epsilon_A(\bar{\nu})d\bar{\nu}}{\bar{\nu}^4} \quad (2)$$

where  $k$  is the orientation factor equal to  $2/3$  as the medium is isotropic,  $n$  is the refractive index of the solvent,  $\epsilon_A(\bar{\nu})$  is the molar extinction coefficient of the acceptor,  $\phi_D$  is the QY of the donor,  $F_D(\bar{\nu})$  is the spectral distribution of the donor normalized to unity,  $N_0$  is Avogadro's number, and  $\bar{\nu}$  is the wavenumber. For more information about the theoretical aspect of this equation, see reference

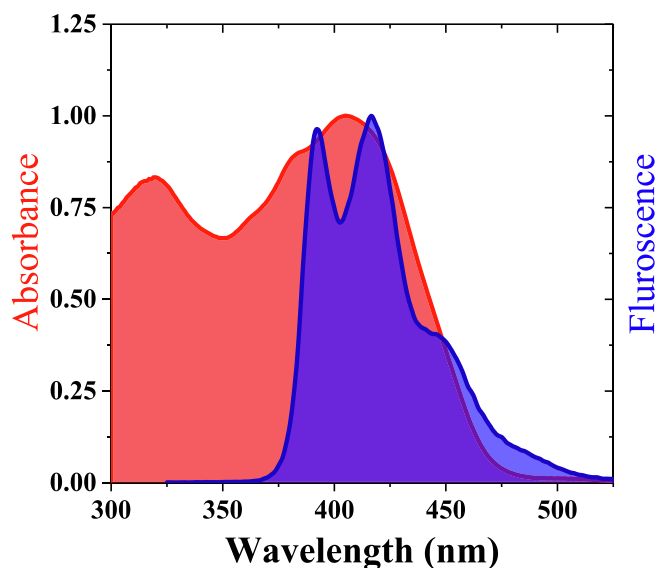
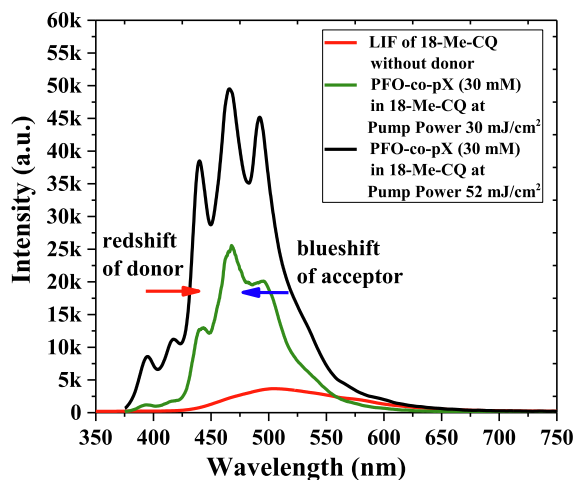


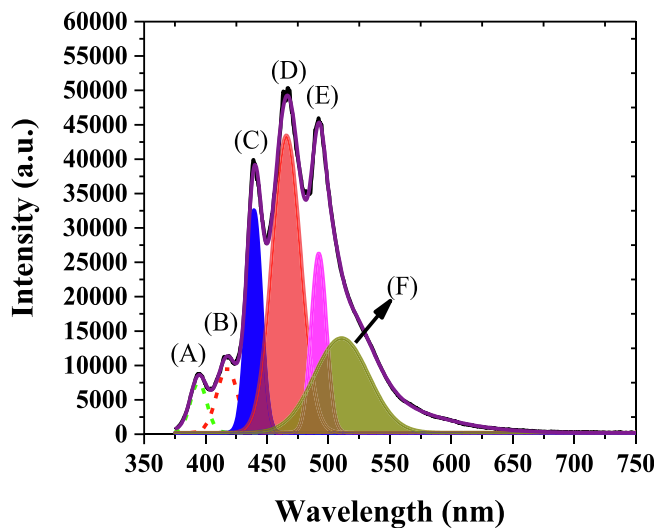
Fig. 8. The normalized absorption of MCQ (acceptor) and fluorescence of PFOPX (donor), the overlap between them and the Stokes' shift before addition of donor.

(Clegg, 2009). The overall spectral overlap was  $6.57 \times 10^{14} M^{-1}cm^{-1}nm^4$ . the calculated extinction co-efficient of MCQ was  $29,980 M^{-1}cm^{-1}$ . The  $R_0$  is calculated using Eq. (2) was equal to 44.09 Å.

Usually, when a FRET occurs between a donor and an acceptor, the donor's fluorescence would be almost extinguished, and only a weak fluorescence would remain, and a blue shifted. Similarly, acceptor fluorescence increases and redshifts. Fig. 9(a) shows the LIF and ASE spectra of pure and mixed solutions of MCQ in toluene. The LIF spectra for the pure MCQ in toluene of concentration of 3.36 mM is very weak with a peak at 505 nm. When 0.5 mL of PFOPX with suitable concentration to form a relative concentration 30 mM was added to 3.36 mM (relative concentration) solution of MCQ volume 3.5 mL. The sample pump energy density of 30 mJ/cm<sup>2</sup> produced very high LIF with a primary peak at 468 nm, blue-shifted from 505 nm. It indicates the occurrence of the FRET between donor and acceptor. For the same mixed solution, the pump energy density was increased to 52 mJ/cm<sup>2</sup>, the appearance of sharp peaks was observed, with five distinctive peaks at 394 nm (A) and 417 nm (B), which is attributed to PFOPX peaks; 440 nm



(a)



(b)

Fig. 9. (a) The LIF and ASE spectra of MCQ and influence of conjugated polymer PFOPX on MCQ under 355 nm laser pumping, (b) Deconvolution of the ASE spectra of MCQ and influence of conjugated polymer PFOPX on MCQ under 355 nm laser pumping.

(C) is due to merging of two vibrations bands of donor and acceptor. The final two peaks at 465 nm (D) and 492 nm (E) were from MCQ, as shown in Fig. 9(b). The band (F) in Fig. 9(b) is due to spectral brooding due to reabsorption. The multipeak analysis (Aljaafreh et al., 2021c) showed in Fig. 7(c) implicated that the peaks at 440 nm (C) and 492 nm (E) had a narrow full-width half maximum of  $13 \pm 2$  and  $14 \pm 2$  nm, which raised from the ASE of MCQ with a divergence of 25 milliradians (mrad). Interestingly, the peak at 465 nm was broad with an FWHM of  $27 \pm 1$  nm did not converge in ASE, and it remained as LIF band which is due to fluorescence spectra interference between PFOPX and MCQ.

#### 4. Conclusions

This work constructs CQs via the cyclization reaction of O-propargylated naphthaldehyde and substituted anilines in good yields. The former starting precursor, O-propargylated naphthaldehyde was derived from 2-hydroxy-1-naphthaldehyde and propargyl bromide. TD-DFT and experimental optical properties of MCQ and PFOPX were studied. The TD-DFT implied that MCQ is a fluorescent compound with a well-defined HOMO–LUMO structure at  $-5.327$  eV and  $-1.836$  eV, respectively, with an energy gap of 3.49 eV in toluene captivity. The TD-DFT simulation of a few monomer-based oligomer models with a truncated tail of PFOPX showed an energy gap of 3.417 eV compared to the experimental value of 3.381 eV with a deviation of 0.036 eV. The experimental studies of MCQ showed solvent-dependent fluorescence peak shifted from  $445 \pm 2$  nm to  $538 \pm 2$  nm for polarity ranging from 0.01 (hexane) to 10.2 (water). Despite the good optical properties, MCQ produced a weak laser-induced fluorescence (LIF) and did not produce amplified spontaneous emission (ASE) for a pump wavelength of 355 nm. The LIF suddenly improved tenfold when PFOPX of concentration 500 nM (50  $\mu$ L) was added to MCQ of 506 mM (3.5 mL) concentration. At the optimal concentration of PFOPX (670 nM) in MCQ solution, the spectrum changed dramatically. The spectrum has five peaks with a LIF in the background, where peaks around 393.5 nm and 417.3 nm attribute to the oligomer; 438.7 nm attributed to a combined fluorescence of oligomer and MCQ; 466.4 nm, and 493.1 nm corresponding to spectral narrowing and ASE from MCQ.

#### Declaration of Competing Interest

The authors declare that they have no known competing financial interests or personal relationships that could have appeared to influence the work reported in this paper.

#### Acknowledgement

This project was funded by the National Plan for Science, Technology, and Innovation (MAARIFAH), King Abdulaziz City for Science and Technology, Kingdom of Saudi Arabia, Award Number (3-17-09-001-0006).

#### Appendix A. Supplementary data

Supplementary data to this article can be found online at <https://doi.org/10.1016/j.jksus.2022.102260>.

#### References

Alfahd, S.A., Rajendra, S.P., Al-Mujammi, W., Devaraj, D., Masilamani, V., AlSalhi, M.S., 2017. An efficient violet Amplified Spontaneous Emission (ASE) from a conjugated polymer (PFO-co-pX) in solution. *Materials* (Basel). 10. <https://doi.org/10.3390/ma10030265>.

Alizadeh, B.H., Ostad, S.N., Foroumadi, A., Amini, M., Dowlatbadi, R., Navidpour, L., Shafiee, A., 2008. Synthesis and cytotoxic activity of novel chromenes. *ARKIVOC* 13, 45–56.

Aljaafreh, M.J., Prasad, S., AlSalhi, M.S., Alahmed, Z.A., 2019. Ultrafast dynamics of laser from green conjugated-oligomer in solution. *Polymer* (Guildf) 169, 106–114. <https://doi.org/10.1016/j.polymer.2019.02.022>.

Aljaafreh, M.J., AlSalhi, M.S., Prasad, S., 2021a. Design of tunable liquid laser based on presence of the conjugated-polymer counter influencing the spectral properties of the oligomer. *Opt. Mater. (Amst)* 111, 110575.

Aljaafreh, M.J., Prasad, S., AlSalhi, M.S., Alhandel, R.H., Alsaigh, R.A., 2021b. TD-DFT Simulation and Experimental Studies of a Mirrorless Lasing of Poly [(9, 9-dioctylfluorenyl-2, 7-diyl)-co-(1, 4-diphenylene-vinylene-2-methoxy-5-(2-ethylhexyloxy)-benzene)]. *Polymers* (Basel) 13, 1430.

Aljaafreh, M.J., Prasad, S., AlSalhi, M.S., Lemmer, U., Alahmed, Z.A., Baloch, M.A., 2021c. Emission dynamics of conjugated oligomer (BECV-DHF)/quantum dot perovskite (CsPbBr<sub>3</sub>) composites in solutions. *Colloids Surf., A Physicochem. Eng. Asp.* 610, 125911.

. *Comprehensive Heterocyclic Chemistry II* 5, 245.

Bani-Yaseen, A.D., Al-Balawi, M., 2014. The solvatochromic, spectral, and geometrical properties of nifenazone: a DFT/TD-DFT and experimental study. *Phys. Chem. Chem. Phys.* 16, 15519–15526.

Bayraktutan, T., Gür, B., Onganer, Y., 2022. A new FRET-based functional chemosensor for fluorometric detection of Fe<sup>3+</sup> and its validation through in silico studies. *J. Mol. Struct.*, 132448.

Belušáková, S., Martínez-Martínez, V., Arbeloa, I.L., Bujdák, J., 2017. Resonance energy transfer between dye molecules in colloids of a layered silicate. The effect of dye surface concentration. *J. Phys. Chem. C* 121, 8300–8309. <https://doi.org/10.1021/acs.jpcc.7b00947>.

Brugel, T.A., Williams, B.W., 1993. Synthesis and characterization of a solvatochromic, lipophilic fluorescent oxazone: 1-Pentyl-7-dimethylamino-3H-phenoxazine-3-one. *J. Fluoresc.* 3, 69–76.

Cai, F., Hou, B., Zhang, S., Chen, H., Ji, S., Shen, X., Liang, H., 2019. A chromenoquinoline-based two-photon fluorescent probe for the highly specific and fast visualization of sulfur dioxide derivatives in living cells and zebrafish. *J. Mater. Chem. B* 7, 2493–2498.

Campbell, N., 1976. *Rodd's Chemistry of Carbon Compounds*, Vol. IVf.

Cerdán, L., Enciso, E., Martín, V., Banuelos, J., López-Arbeloa, I., Costela, A., García-Moreno, I., 2012. FRET-assisted laser emission in colloidal suspensions of dye-doped latex nanoparticles. *Nat. Photonics* 6, 621–626.

Chang, S., Grubbs, R.H., 1998. A highly efficient and practical synthesis of chromene derivatives using ring-closing olefin metathesis. *J. Org. Chem.* 63, 864–866.

Cho, S.H., Cho, J.Y., Kang, S.E., Hong, Y.K., Ahn, D.H., 2008. Antioxidant activity of mojabanchromanol, a novel chromene, isolated from brown alga *Sargassum siliquastrum*. *J. Environ. Biol.* 29, 479–484.

Civcir, P.Ü., Özen, E., Karadeniz, C., 2020. Narrow-energy gap conjugated polymers based on benzobisthiadiazole and thiadiazoloquinoline: DFT and TDDFT study. *J. Mol. Model.* 26, 1–18.

Clegg, R.M., 1995. Fluorescence resonance energy transfer. *Curr. Opin. Biotechnol.* 6, 103–110.

Clegg, R.M., 2009. Chapter 1 Förster resonance energy transfer-FRET what is it, why do it, and how it's done. *Lab. Tech. Biochem. Mol. Biol.* [https://doi.org/10.1016/S0075-7535\(08\)00001-6](https://doi.org/10.1016/S0075-7535(08)00001-6).

Coghlan, M.J., Kym, P.R., Elmore, S.W., Wang, A.X., Luly, J.R., Wilcox, D., Stashko, M., Lin, C.-W., Miner, J., Tyree, C., 2001. Synthesis and characterization of non-steroidal ligands for the glucocorticoid receptor: selective quinoline derivatives with prednisolone-equivalent functional activity. *J. Med. Chem.* 44, 2879–2885.

Conti, C., Desideri, N., 2009. Synthesis and antirhinovirus activity of new 3-benzyl chromene and chroman derivatives. *Bioorg. Med. Chem.* 17, 3720–3727.

Duan, Y., Ding, G., Yao, M., Wang, Q., Guo, H., Wang, X., Zhang, Y., Li, J., Li, X., Qin, X., 2020. Novel triphenylamine-based fluorescent chemo-sensors for fast detection of thiophenols in vitro and in vivo. *Spectrochim. Acta Part A Mol. Biomol. Spectrosc.* 236, 118348.

Frisch, M.J., Trucks, G.W., Schlegel, H.B., Scuseria, G.E., Robb, M.A., Cheeseman, J.R., Scalmani, G., Barone, V., Petersson, G.A., Nakatsuji, H., 2016. *Gaussian 16*.

Geng, Y., Tian, H., Yang, L., Liu, X., Song, X., 2018. An aqueous methylated chromenoquinoline-based fluorescent probe for instantaneous sensing of thiophenol with a red emission and a large Stokes shift. *Sensors Actuators B Chem.* 273, 1670–1675.

Ghatak, C., Rao, V.G., Pramanik, R., Sarkar, S., Sarkar, N., 2011. The effect of membrane fluidity on FRET parameters: an energy transfer study inside small unilamellar vesicle. *Phys. Chem. Chem. Phys.* 13, 3711–3720.

Gopalakrishnan, S., Vijayakumar, S., Shankar, R., 2018. DFT/TD-DFT study on halogen doping and solvent contributions to the structural and optoelectronic properties of poly [3, 6-carbazole] and poly [indolo (3, 2-b)-carbazole]. *Struct. Chem.* 29, 1775–1796.

Heyduk, T., 2002. Measuring protein conformational changes by FRET/LRET. *Curr. Opin. Biotechnol.* 13, 292–296.

Hrdlovic, P., Donovalova, J., Stankovicova, H., Gaplovsky, A., 2010. Influence of polarity of solvents on the spectral properties of bichromophoric coumarins. *Molecules* 15, 8915–8932.

Hussain, S.A., 2009. *An Introduction to Fluorescence Resonance Energy Transfer (FRET)*.

Kand, D., Kalle, A.M., Varma, S.J., Talukdar, P., 2012. A chromenoquinoline-based fluorescent off-on thiol probe for bioimaging. *Chem. Commun.* 48, 2722–2724.

Kenworthy, A.K., 2001. Imaging protein-protein interactions using fluorescence resonance energy transfer microscopy. *Methods* 24, 289–296.

- Kjer, J., Wray, V., Edrada-Ebel, R., Ebel, R., Pretsch, A., Lin, W., Proksch, P., 2009. Xanaleric acids I and II and related phenolic compounds from an endophytic *Alternaria* sp. isolated from the mangrove plant *Sonneratia alba*. *J. Nat. Prod.* 72, 2053–2057.
- Kleschick, W.A., Heathcock, C.H., 1978. Synthesis and chemistry of ethyl 2-diethylphosphonoacrylate. *J. Org. Chem.* 43, 1256–1259.
- Ku, Y.-Y., Grieme, T., Raje, P., Sharma, P., Morton, H.E., Rozema, M., King, S.A., 2003. A practical and scaleable synthesis of A-224817.0, a novel nonsteroidal ligand for the glucocorticoid receptor. *J. Org. Chem.* 68, 3238–3240.
- Lakshmidevi, V., Parvathi, P., Venkataraman, A., 2017. Effect of solvent polarity on fluorescence spectra of camphor sulphonic acid doped polyaniline. *Mad. J. Anal. Sci. Instrum.* 2, 21–24.
- Liu, X., Li, Y., Ren, X., Yang, Q., Su, Y., He, L., Song, X., 2018. Methylated chromenoquinoline dyes: synthesis, optical properties, and application for mitochondrial labeling. *Chem. Commun.* 54, 1509–1512.
- McCormick, T.M., Bridges, C.R., Carrera, E.I., Dicarmine, P.M., Gibson, G.L., Hollinger, J., Kozycz, L.M., Seferos, D.S., 2013. Conjugated polymers: Evaluating DFT methods for more accurate orbital energy modeling. *Macromolecules* 46, 3879–3886.
- Minami, T., Sukanuma, H., Agawa, T., 1978. Synthesis and reactions of vinylphosphonates bearing electronegative substituents. *Chem. Lett.* 7, 285–288.
- Nicolaou, K.C., Pfefferkorn, J.A., Roecker, A.J., Cao, G.-Q., Barluenga, S., Mitchell, H.J., 2000. Natural product-like combinatorial libraries based on privileged structures. 1. General principles and solid-phase synthesis of benzopyrans. *J. Am. Chem. Soc.* 122, 9939–9953.
- Prasad, S., Aljaafreh, M.J., Alsalhi, M.S., 2020. Time-resolved spectroscopy of radiative energy transfer between a conjugated oligomer and polymer in solution. *Spectrochim. Acta Part A Mol. Biomol. Spectrosc.* 232, 118151. <https://doi.org/10.1016/j.SAA.2020.118151>.
- Qiao, L., Yang, Y., Cai, J., Lv, X., Hao, J., Li, Y., 2022. Long wavelength emission fluorescent probe for highly selective detection of cysteine in living cells. *Spectrochim. Acta Part A Mol. Biomol. Spectrosc.* 264, 120247.
- Ramesh, S., Gaddam, V., Nagarajan, R., 2010. A flexible approach to the chromenoquinolines under copper/Lewis acid catalysis. *Synlett* 2010, 757–760.
- Sami, I., Kar, G.K., Ray, J.K., 1992. Synthesis of polycyclic oxa-coumarins, potential antitumour agents and a short and convenient synthesis of naphthopyranoquinolines from naphthopyran chloroaldehydes. *Tetrahedron* 48, 5199–5208.
- Sharghi, H., Khalifeh, R., Rashidi, Z., 2013. Synthesis of chromeno [3, 4- $\{b\}$ ] quinoline derivatives by heterogeneous [Cu (II) BHPPDAH] catalyst without being immobilized on any support under mild conditions using PEG 300 as green solvent. *Mol. Divers.* 17, 721–730.
- Tangmouo, J.G., Meli, A.L., Komguem, J., Kuete, V., Ngounou, F.N., Lontsi, D., Beng, V. P., Choudhary, M.I., Sondengam, B.L., 2006. Crassiflorone, a new naphthoquinone from *Diospyros crassiflora* (Hien). *Tetrahedron Lett.* 47, 3067–3070.
- Vu, A.T., Campbell, A.N., Harris, H.A., Unwalla, R.J., Manas, E.S., Mewshaw, R.E., 2007. ER $\beta$  ligands. Part 6: 6H-Chromeno [4,3- $\{b\}$ ] quinolines as a new series of estrogen receptor  $\beta$ -selective ligands. *Bioorg. Med. Chem. Lett.* 17, 4053–4056.
- Wang, Q., Finn, M.G., 2000. 2H-chromenes from salicylaldehydes by a catalytic petasis reaction. *Org. Lett.* 2, 4063–4065.
- Yadav, P., Lal, K., Kumar, L., Kumar, A., Kumar, A., Paul, A.K., Kumar, R., 2018. Synthesis, crystal structure and antimicrobial potential of some fluorinated chalcone-1,2,3-triazole conjugates. *Eur. J. Med. Chem.* 155, 263–274.
- Zhi, L., Tegley, C.M., Pio, B., Edwards, J.P., Motamedi, M., Jones, T.K., Marschke, K.B., Mais, D.E., Risek, B., Schrader, W.T., 2003. 5-Benzylidene-1,2-dihydrochromeno [3,4- $\{f\}$ ] quinolines as selective progesterone receptor modulators. *J. Med. Chem.* 46, 4104–4112.